Why Charged Molecules Move Across a Temperature Gradient: The Role of Electric Fields

Maren Reichl, Mario Herzog, Alexandra Götz, and Dieter Braun[*]

*Systems Biophysics, Physics Department, Nanosystems Initiative Munich and
Center for NanoScience Ludwig-Maximilians-Universität München, Amalienstrasse 54, 80799 München, Germany*

Methods to move solvated molecules are rare. Apart from electric fields, only thermal gradients are effective enough to move molecules inside a fluid. This effect is termed thermophoresis, and the underlying mechanisms are still poorly understood. Nevertheless, it is successfully used to quantify biomolecule binding in complex liquids. Here we show experiments that reveal that thermophoresis in water is dominated by two electric fields, both established by the salt ions of the solution. A local field around the molecule drives molecules along an energy gradient, whereas a global field moves the molecules by a combined thermoelectrophoresis mechanism known as the Seebeck effect. Both mechanisms combined predict the thermophoresis of DNA and RNA polymers for a wide range of experimental parameters. For example, we correctly predict a complex, nonlinear size transition, a salt-species-dependent offset, a maximum of thermophoresis over temperature, and the dependence of thermophoresis on the molecule concentration.

Introduction.—Thermophoresis is the motion of molecules induced by a temperature gradient, often also referred to as the Soret effect, thermodiffusion, or thermal diffusion. Typically, the molecule concentration depletes at positions of locally enhanced temperature. The strength of depletion is parameterized by the Soret coefficient S_T [1,2] and given by $c = c_0 \exp[-S_T(T - T_0)]$ with the depleted concentration c at varying temperature T at a bulk concentration and temperature c_0 and T_0, respectively. Predictive models to calculate S_T based on molecule parameters are missing. Often, the nonequilibrium analogy between thermophoresis and electrophoresis is assumed while a local equilibrium considerations are not considered.

For the last 3 years, a growing number of biologists have used thermophoresis as a method [3,4] for quantifying biomolecule binding [5–10]. Also, central questions of molecular evolution were addressed by thermophoretic traps [11–13]. Despite the general interest in the topic, the above applications of thermophoresis are missing a solid theoretical foundation at the moment.

To approach the problem, systematic experiments over a large parameter space are required. Polymers in nonaqueous solutions show a clear scaling behavior with molecular weight [14] and isotope composition [15]. The mass dependence of thermophoresis in silica melts [16] suggested a quantum mechanical treatment [17,18]. Polystyrene beads and long double-stranded DNA of various size were studied [19,20], suggesting a plate capacitor model [21]. Size-dependent measurements of polystyrene beads at constant Debye length, however, disputed the results [22].

Here, single- and double-stranded DNA and RNA of different lengths were measured for various salt concentrations, salt species, and temperatures. The experiments test the size transition of the capacitor model, especially for Debye lengths larger than the molecule size. In addition, they probe a thermoelectric Seebeck contribution, suggested by experiments [23] and theoretical treatments [24,25]. Oligonucleotides offer a precise length definition, excellent purity, and fluorescence-based measurements at low concentrations. Many molecular parameters are known for oligonucleotides.

Theory.—In the following, thermophoresis is described with a combination of four molecular mechanisms, fully described in the Supplemental Material Sec. S1 [26]:

$$S_T = S_T^{CM} + S_T^{EL} + S_T^{NI} + 1/T \qquad (1)$$

The capacitor model [21] described in Fig. 1(a) leads to

$$S_T^{CM} \frac{R}{Z_{\text{eff}}^2} = \frac{e^2 R/\lambda_{DH}}{16\pi k_B T^2 \varepsilon_r \varepsilon_0 (1 + R/\lambda_{DH})^2}$$
$$\times \left(1 - \frac{\partial \ln \rho(T)}{\partial \ln T} - \frac{\partial \ln \varepsilon_r(T)}{\partial \ln T}\left(1 + \frac{2\lambda_{DH}}{R}\right)\right). \qquad (2)$$

As seen, the right-hand side only depends on constants and a rescaled Debye length λ_{DH}/R with the hydrodynamic molecule radius R. The Seebeck effect is visualized in Fig. 1(b) and is derived analogously to the monovalent salt cases [24,25]:
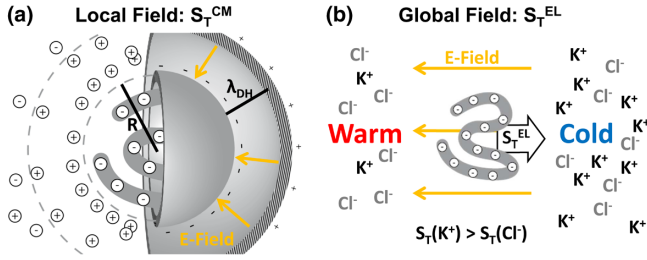
FIG. 1 (color online). Local and global electric fields move molecules along a temperature gradient. (a) Around a charged molecule, dissolved ions form a shielding capacitor with Debye length λ_{DH}. The energy stored in the capacitor decreases in the cold and leads to a positive Soret coefficient S_T^{CM}. For molecules with radius R smaller than the Debye length λ_{DH}, the radial capacitor can be approximated as a point charge; for larger molecules, it can be approximated as a plate capacitor. The result is a nonlinear size transition depending on λ_{DH}/R. (b) The differential Soret coefficients of ions in solution, here K$^+$ and Cl$^-$, create a global electric field. The resulting electrophoresis cannot be readily distinguished from thermophoresis. This Seebeck effect results in an ion-species-dependent offset S_T^{EL} that is independent of the Debye length for the used experimental conditions.

$$S_T^{EL} = -\frac{k_B T \mu_{DNA}}{e \, D_{DNA}} \frac{\sum_i z_i c_i S_{Ti}}{\sum_i z_i^2 c_i}. \qquad (3)$$

Finally, the temperature dependence of nonionic contributions are fitted empirically [27] according to

$$S_T^{NI} = S_T^\infty \left[1 - \exp\left(\frac{T^* - T}{T_0}\right)\right] \qquad (4)$$

The small contribution $1/T$ is based on the temperature dependence of the diffusion coefficient.

Results.—We first test the capacitor model contribution S_T^{CM}. Single-stranded DNA and RNA form a spherical coil due to their short persistence length. For elongated shapes, the dependence on λ_{DH} is expected to be very similar [28]. Inside the hydrodynamic radius R, adsorbed ions reduce the bare charge to the effective charge Z_{eff}. Toward the periphery, the molecule is shielded within the Debye length λ_{DH} created by the ions in solution [Fig. 1(a)]. Depending on the size ratio λ_{DH}/R, the capacitor can be approximated as a plate capacitor when $\lambda_{DH} \ll R$. This plate capacitor case was studied previously [29], and S_T^{CM} rises linearly with λ_{DH}. For the size regime $\lambda_{DH} \ll R$, the shielding capacitor becomes a point charge, and according Eq. (2), the Soret coefficient should saturate toward a constant value.

As shown in Fig. 2(a), the measurements confirm this nontrivial prediction of the capacitor model without the need to fit of the molecule or its effective charge. We measured single-stranded DNA with lengths of 2, 5, 10, 22, 50, and 80 bases. For short DNA, a transition of the measured Soret coefficients toward a constant value is
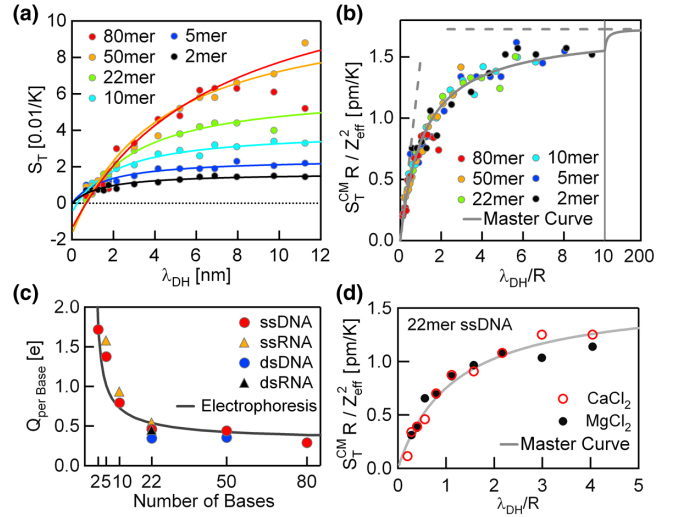

FIG. 2 (color online). Nonlinear size transition of capacitive thermophoresis. (a) The Soret coefficient S_T is measured for single-stranded DNA with lengths of 2, 5, 10, 22, 50, and 80 bases and plotted against Debye length λ_{DH} at 15°C. The radius R is measured from diffusion; the effective charge describes the amplitude, and a constant offset $S_T(\lambda_{DH} = 0) = S_T^{EL} + S_T^{NI} + 1/T$ is determined. (b) After rescaling the data according to Eq. (2), the measurements fall onto a single master curve and confirm in detail the size transition of the capacitor model. Broken lines denote the limiting cases for $\lambda_{DH} \ll R$ and $\lambda_{DH} \gg R$. (c) The effective charge per base fitted from the capacitor model decreases with increasing length. The number of bases is used as a measure of molecule length; thus, only half of the bases of the double stranded species is counted. It matches the effective charge known from electrophoresis shown as a solid line [32]. (d) Thermophoresis measurements using divalent salt ions equally follow the same capacitor model.

found at small λ_{DH}, whereas longer DNA first rises linearly and bends but does not fully saturate in the tested λ_{DH} regime. The data can be fitted by Eq. (2) with the hydrodynamic radius R measured through the diffusion coefficient (Supplemental Material S3 [26]). The amplitude of the curve is adjusted by the effective charge number Z_{eff} and later compared to the effective charge known from electrophoresis. Contributions from the capacitor model vanish for $\lambda_{DH} = 0$, and thermophoresis is given by $S_T^{EL} + S_T^{NI} + 1/T$, which does not depend on λ_{DH}. After subtracting this offset, the data are rescaled by Z_{eff}^2/R and plotted against a rescaled Debye-axis λ_{DH}/R with the measured radius R. All measurements fall onto the single master curve of the capacitor model Eq. (2) [Fig. 2(b)].

Initially, the effective charge number Z_{eff} is a fitting parameter of the capacitor model. To compare with electrophoresis, it is divided by the number of bases (or base pairs for the double stranded species) and plotted versus DNA length in Fig. 2(c). It decreases with DNA length. This effect is known for DNA from electrophoresis and attributed to Manning condensation [30–32]. A most recent model using multiparticle collision dynamics [33] is plotted

as a solid line. The effective charge from electrophoresis matches the effective charge determined from thermophoresis by the capacitor model remarkably well.

Very similar results are found for single-stranded RNA (Supplemental Material S3 [26]). As known from electrophoresis, the effective charge of double-stranded DNA or RNA does not differ much from their single-stranded versions [31]. The same is found for the charges determined from thermophoresis. The 80mer deviates for large λ_{DH}, marking the breakdown of the internal shielding approximation. To test the generality of the approach, we measured 22mer single-stranded DNA using the divalent salts $CaCl_2$ and $MgCl_2$ [Fig. 2(d)]. The Debye length includes now the different contributions from the used monovalent and divalent ion concentrations. As seen, the capacitor model equally describes the measurements for divalent ions. The effective charge per base is twofold smaller (0.2e per base), but a similar decrease of the electric mobility for higher valent salts is known [34]. Overall, the temperature dependence of the energy stored in the ionic shielding describes the salt-concentration-dependent contribution in thermophoresis remarkably well.

Since the pioneering salt-species-dependent measurement of Putnam and Cahill [23], a contribution to thermophoresis from the Seebeck effect was suspected but not demonstrated without fitting parameters. Salt ions follow a differential thermophoretic pattern, create an electric field, and move molecules by electrophoresis. Under our experimental conditions, we expect that this thermoelectric effect leads to a salt-species-dependent but salt-concentration-independent offset of the capacitor model (Supplemental Material S5 [26]). Neither the large Soret coefficient of OH^-, H_3O^+ nor the highly charged DNA itself contributes significantly as the millimolar salt concentrations dominate the sums in Eq. (3).

The measurement of negatively charged 2mer, 22mer, and 80mer single-stranded DNA and of positively charge rhodamine 6G for varying concentrations of KBr, KCl, KF, KI, NaBr, NaCl, NaF, NaI, LiBr, LiCl, and LiI is shown in the Supplement Material S5 [26]. The dependence of S_T on the Debye length can be fully described by the capacitor model, but an additional offset of the Soret coefficient is found that depends on the salt species. In Fig. 3(a), we compare the offset minus $1/T$ minus a constant S_T^{NI} to the Seebeck theory using published Soret coefficients of the salt species [36,37]. A very convincing match between the measured S_T^{EL} and the theoretical Seebeck effect is found.

We check the model internally by comparing the charge of the capacitor model [Fig. 2(c)] with the charge derived from the Seebeck effect. The electric mobility is fitted from the differential thermophoresis and reveals $\mu_{DNA} = -1.2 \pm 0.13$, -2.6 ± 0.24, and $-1.2 \pm 0.13 \times 10^{-8}$ m^2/Vs for the 2mer, 22mer, and 80mer, consistent with literature values (see the Supplemental Material S5 [26]). Note that the Seebeck effect depends on the sign
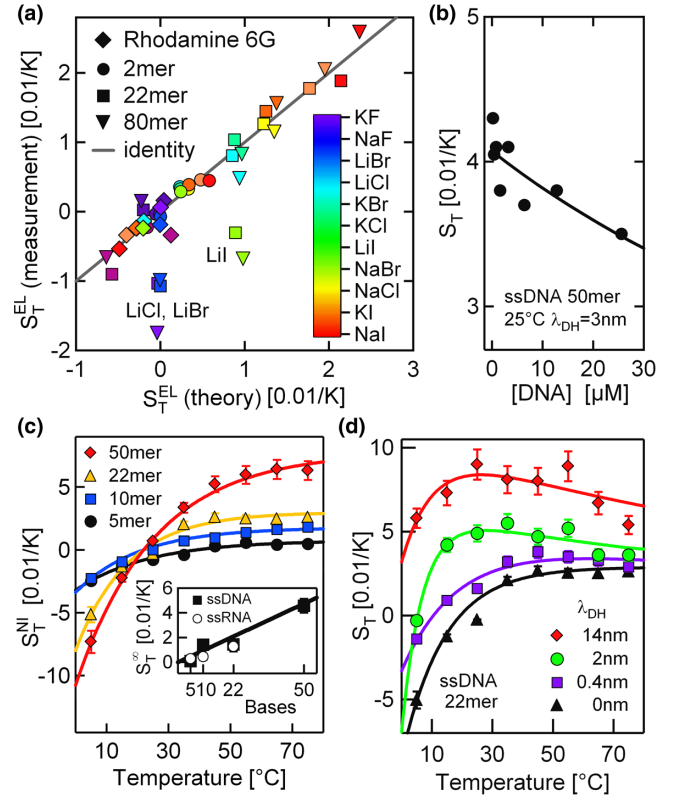

FIG. 3 (color online). Seebeck contribution and dependence on concentration and temperature. (a) The Seebeck contribution S_T^{EL} is extracted from salt-species-dependent measurements (Supplemental Material S5 [26]) by extrapolating to $\lambda_{DH} = 0$, subtracting $1/T$, and removing the nonionic, molecule-specific contribution S_T^{NI} according to Eq. (1). The theoretical Seebeck contribution [Eq. (3)] matches the experimental S_T^{EL} for positively charged rhodamine 6G and negatively charged 2mer, 22mer, and 80mer ssDNA, with small deviations of lithium salts for 22mer and 80mer. (b) The DNA concentration dependence of thermophoresis matches the prediction based on the Seebeck effect. (c) After subtracting S_T^{CM}, S_T^{EL}, and $1/T$ from the measurements, the remaining nonionic contribution S_T^{NI} matches the empirical Eq. (4) proposed by Piazza [35]. Its magnitude S_T^∞ scales linearly with DNA length (inset). (d) Ionic thermophoresis decreases with temperature [Eq. (2)] but increases with the nonionic contribution [Eq. (4)]. Their combination directly explains the nontrivial maximum of thermophoresis at intermediate temperatures.

of the charge, in contrast to S_T^{CM}. As predicted, measurements of the positively charged dye rhodamine 6G invert the order of the salt species.

Interestingly, the measured DNA concentration dependence of thermophoresis [Fig. 3(b)] can be fully explained by the Seebeck effect and the capacitor model (Supplemental Material S6 [26]). The oligonucleotide charge does not change between the two relevant pK_a values of oligonucleotides above 4.3 or below 8.7 [38]. In confirmation of the model, the Soret coefficient of DNA is constant within a pH of 5–9 (Supplemental Material S4 [26]). Outside this pH range, thermophoresis drops

as expected from the reduced nucleotide charge. This also supports the theoretically expected negligible contribution to the Seebeck effect from OH^- and H_3O^+ ions (Supplemental Material S5 [26]). While OH^- and H_3O^+ ions have large Soret coefficients, their micromolar concentration near neutral pH cannot compete against the millimolar salt concentrations in Eq. (3). These results do not contradict reports measuring without buffer at high pH [39]. On the same grounds, a possible constant Seebeck contribution from the unknown Soret coefficient of the TRIS buffer was neglected.

After subtracting the Seebeck effect S_T^{EL}, subtracting the ideal gas contribution $1/T$, and extrapolating the capacitor model S_T^{CM} toward $\lambda_{DH} \to 0$, we are left with the nonionic contribution S_T^{NI} [Eq. (1)]. As seen in Fig. 3(c), the measured S_T^{NI} rises characteristically over temperature and can be fitted with the empirical Eq. (4). As shown in the inset, the nonionic amplitude S_T^∞ shows a linear dependence on DNA (or RNA) length as expected for a local, molecule-solvent interaction across the area of a thin tube around the polymer.

The temperature dependence of thermophoresis in Fig. 3(d) shows a maximum that is increasingly prominent for increasing Debye length. This nontrivial dependence is readily described by Eq. (1). Since the condensed charges do not depend significantly on temperature, S_T^{CM} decreases as the temperature increases according to Eq. (2). The nonionic contribution S_T^{NI} rises over the temperature [Eq. (4)]. The small Seebeck term S_T^{EL} is largely temperature independent. Without additional parameters, the measurements are fully described [Fig. 3(d), lines]. As shown in the Supplemental Material S7 [26], two-dimensional measurements over Debye length and temperature are fully predicted by Eq. (1).

Discussion.—Our analysis of the experiments suggests that a thermodynamic approach is valid for thermophoresis. The total energy of a molecule differs along a thermal gradient, in contrast to electrophoresis where the fully shielded molecule shows no potential energy difference in an electric field. Typical for thermophoresis and including our measurements, depleted concentrations never drop below 50% of the bulk concentration. The diffusion back into the heated region can be achieved by thermodynamic fluctuations over the time of the experiment. The Peclet number (Pe) of the molecules, also termed the Brenner number, is smaller than one even for the largest 80mer ssDNA used in this work, $Pe = R S_T \nabla T = 10\ \text{nm} \times 0.0001\ \text{K}^{-1} \times 5\ \text{K}/50\ \mu\text{m} = 10^{-4}$, documenting the diffusion-dominated molecule motion. All of the above substantiate a local equilibrium approach to thermophoresis. Fluorescence imaging allows us to measure at a 1-μM molecule concentration, more than 3 orders of magnitude smaller than the overlap concentration c^*. The average molecule distance is 120 nm, more than tenfold larger than the diameter of the largest measured molecule. Therefore,

we do not include concentration-dependent effects in Eq. (1) [40,41].

Understanding thermophoresis on a molecular level is highly beneficial to use thermophoresis in biomolecular binding studies [3–10,42]. Using the successful model of thermophoresis, the changes of S_T upon molecule binding can be quantitatively predicted. Also, since the electrophoretic mobility is measured all optically by measuring thermophoresis for different salt species [Fig. 3(a)], direct inference on the sign and magnitude of a charged molecule becomes possible.

*Corresponding author.
dieter.braun@lmu.de

[1] C. Ludwig, *Diffusion Zwischen Ungleich Erwärmten Orten Gleich Zusammengesetzter Lösung* (Akademie der Wissenschaften, Wien, 1856).
[2] C. Soret, Arch. Geneve 3 **48** (1879).
[3] P. Baaske, C. J. Wienken, P. Reineck, S. Duhr, and D. Braun, Angew. Chem., Int. Ed. Engl. **49**, 2238 (2010).
[4] C. J. Wienken, P. Baaske, U. Rothbauer, D. Braun, and S. Duhr, Nat. Commun. **1**, 100 (2010).
[5] S. Bhogaraju et al., Science **341**, 1009 (2013).
[6] X. Xiong et al., Nature (London) **497**, 392 (2013).
[7] X. Shang, F. Marchioni, C. R. Evelyn, N. Sipes, X. Zhou, W. Seibel, M. Wortman, and Y. Zheng, Proc. Natl. Acad. Sci. U.S.A. **110**, 3155 (2013).
[8] C. G. Alexander, M. C. Jurgens, D. A. Shepherd, S. M. V. Freund, A. E. Ashcroft, and N. Ferguson, Proc. Natl. Acad. Sci. U.S.A. **110**, E2782 (2013).
[9] M. Gertz, F. Fischer, G. T. T. Nguyen, M. Lakshminarasimhan, M. Schutkowski, M. Weyand, and C. Steegborn, Proc. Natl. Acad. Sci. U.S.A. **110**, E2772 (2013).
[10] T. Cherrier et al., Proc. Natl. Acad. Sci. U.S.A. **110**, 12 655 (2013).
[11] P. Baaske, F. M. Weinert, S. Duhr, K. H. Lemke, M. J. Russell, and D. Braun, Proc. Natl. Acad. Sci. U.S.A. **104**, 9346 (2007).
[12] C. B. Mast and D. Braun, Phys. Rev. Lett. **104**, 188102 (2010).
[13] C. B. Mast, S. Schink, U. Gerland, and D. Braun, Proc. Natl. Acad. Sci. U.S.A. **110**, 8030 (2013).
[14] D. Stadelmaier and W. Köhler, Macromolecules **42**, 9147 (2009).

[15] G. Wittko and W. Köhler, J. Chem. Phys. **123**, 014506 (2005).

[16] F. Huang, P. Chakraborty, C. C. Lundstrom, C. Holmden, J. J. G. Glessner, S. W. Kieffer, and C. E. Lesher, Nature (London) **464**, 396 (2010).

[17] G. Dominguez, G. Wilkins, and M. H. Thiemens, Nature (London) **473**, 70 (2011).

[18] S. Hartmann, W. Köhler, and K. I. Morozov, Soft Matter **8**, 1355 (2012).

[19] S. Duhr and D. Braun, Proc. Natl. Acad. Sci. U.S.A. **103**, 19 678 (2006).

[20] P. Reineck, C. J. Wienken, and D. Braun, Electrophoresis **31**, 279 (2010).

[21] J. K. G. Dhont, S. Wiegand, S. Duhr, and D. Braun, Langmuir **23**, 1674 (2007).

[22] M. Braibanti, D. Vigolo, and R. Piazza, Phys. Rev. Lett. **100**, 108303 (2008).

[23] S. A. Putnam and D. G. Cahill, Langmuir **21**, 5317 (2005).

[24] G. Guthrie, J. N. Wilson, and V. Schomaker, J. Chem. Phys. **17**, 310 (1949).

[25] A. Würger, Phys. Rev. Lett. **101**, 108302 (2008).

[26] See Supplemental Material at http://link.aps.org/supplemental/10.1103/PhysRevLett.112.198101 for more information on calculations, simulations, measurements and discussion details.

[27] S. Iacopini, R. Rusconi, and R. Piazza, Eur. Phys. J. E **19**, 59 (2006).

[28] Z. Wang, H. Kriegs, J. Buitenhuis, J. K. G. Dhont, and S. Wiegand, Soft Matter **9**, 8697 (2013).

[29] S. Duhr and D. Braun, Phys. Rev. Lett. **96**, 168301 (2006).

[30] D. A. Hoagland, E. Arvanitidou, and C. Welch, Macromolecules **32**, 6180 (1999).

[31] E. Stellwagen, Y. Lu, and N. C. Stellwagen, Biochemistry **42**, 11 745 (2003).

[32] K. Grass, U. Böhme, U. Scheler, H. Cottet, and C. Holm, Phys. Rev. Lett. **100**, 096104 (2008).

[33] O. A. Hickey, T. N. Shendruk, J. L. Harden, and G. W. Slater, Phys. Rev. Lett. **109**, 098302 (2012).

[34] R. W. O'Brien and L. R. White, J. Chem. Soc., Faraday Trans. 2 **74**, 1607 (1978).

[35] S. Iacopini and R. Piazza, Europhys. Lett. **63**, 247 (2003).

[36] N. Takeyama and K. Nakashima, J. Solution Chem. **17**, 305 (1988).

[37] C. J. Petit, M.-H. Hwang, and J.-L. Lin, Int. J. Thermophys. **7**, 687 (1986).

[38] S. Chatterjee, W. Pathmasiri, O. Plashkevych, D. Honcharenko, O. P. Varghese, M. Maiti, and J. Chattopadhyaya, Org. Biomol. Chem. **4**, 1675 (2006).

[39] D. Vigolo, S. Buzzaccaro, and R. Piazza, Langmuir **26**, 7792 (2010).

[40] Y. T. Maeda, T. Tlusty, and A. Libchaber, Proc. Natl. Acad. Sci. U.S.A. **109**, 17 972 (2012).

[41] H.-R. Jiang, H. Wada, N. Yoshinaga, and M. Sano, Phys. Rev. Lett. **102**, 208301 (2009).

[42] S. Lippok, S. A. I. Seidel, S. Duhr, K. Uhland, H.-P. Holthoff, D. Jenne, and D. Braun, Anal. Chem. **84**, 3523 (2012).